

Inelastic seismic response of adjacent buildings linked by fluid dampers

Y. L. Xu[†] and Z. Yang[‡]

Department of Civil and Structural Engineering, The Hong Kong Polytechnic University, Hung Hom, Kowloon, Hong Kong, China

X. L. Lu[†]

Research Institute of Structural Engineering and Disaster Reduction, Tongji University, Shanghai 200092, China

(Received November 27, 2001, Accepted March 18, 2003)

Abstract. Using fluid dampers to connect adjacent buildings for enhancing their seismic resistant performance has been recently investigated but limited to linear elastic adjacent buildings only. This paper presents a study of inelastic seismic response of adjacent buildings linked by fluid dampers. A nonlinear finite element planar model using plastic beam element is first constructed to simulate two steel frames connected by fluid dampers. Computed linear elastic seismic responses of the two steel frames with and without fluid dampers under moderate seismic events are then compared with the experimental results obtained from shaking table tests. Finally, elastic-plastic seismic responses of the two steel frames with and without fluid dampers are extensively computed, and the fluid damper performance on controlling inelastic seismic response of the two steel frames is assessed. The effects of the fundamental frequency ratio and structural damping ratio of the two steel frames on the damper performance are also examined. The results show that not only in linear elastic stage but also in inelastic stage, the seismic resistant performance of the two steel frames of different fundamental frequencies can be significantly enhanced if they are properly linked by fluid dampers of appropriate parameters.

Key words: adjacent buildings; fluid damper; inelastic seismic response; plastic beam element; numerical simulation; experimental comparison.

1. Introduction

Buildings in a modern city are often built closely to each other because of limited availability of land and preference for centralized services. Although most of these buildings are separated without any structural connections, some of them are linked together in different ways to meet requirements such as architectural function and structural performance. For instance, some of adjacent buildings are linked by sky bridges at several locations to provide a horizontal

[†] Professor

[‡] Research Assistant

transportation system for access to the two buildings. Some of tall buildings are built with podium structures to achieve a large open space for parking, shops, restaurants and hotel lobbies. The concept of linking adjacent buildings or connecting podium structures to a main building using passive dampers, semi-active dampers, or active dampers has been thus proposed to improve their seismic resistant performance.

The investigation of using passive dampers to connect adjacent buildings for enhancing their seismic resistant performance has been carried out by Kobori *et al.* (1988), Luco *et al.* (1998), and Zhang and Xu (1999) among others. The use of active actuators to link a group of buildings to reduce their seismic responses has been examined by Yamada *et al.* (1994), Seto and Matsumoto (1996), and others. Klein and Healy (1985) and Christenson *et al.* (1999) respectively scrutinized the performance of semi-active control devices for seismic response mitigation of adjacent buildings. The experimental investigations of adjacent buildings linked by fluid dampers have been also executed by Xu *et al.* (1999) for the buildings under harmonic excitation and by Yang *et al.* (2002) for the buildings under seismic excitation through shaking table tests. All these investigations demonstrated that the use of dampers to link adjacent buildings of different fundamental frequencies could significantly reduce seismic response of either building if the locations and parameters of dampers were appropriately selected. All these investigations are limited to linear elastic adjacent buildings with the assumption that either the intensity of ground motion is moderate or because of the installation of dampers the energy dissipation capacity of the buildings is enhanced enough to keep the buildings elastic. However, this may not be the case for adjacent buildings located in strong seismic zones or for inadequate energy dissipation capacity of control devices used to link adjacent buildings.

This paper therefore focuses on inelastic seismic response and behavior of adjacent buildings linked by fluid dampers. The background of the establishment of a nonlinear finite element model using plastic beam element to simulate two steel frames connected by fluid damper is first given. Followed is a procedure for solving the nonlinear equations of motion of the structural-damper system. Computed linear elastic seismic responses of the two steel frames with and without fluid dampers under moderate seismic events are then compared with the experimental results obtained from shaking table tests. Finally, elastic-plastic seismic response and behavior of the two steel frames with and without fluid dampers are investigated in terms of response time history, the maximum story drift profile, and hysteretic loops of structural members. The fluid damper performance on controlling inelastic seismic response of the two steel frames and the effects of the fundamental frequency ratio and structural damping ratio of the two steel frames on the fluid damper performance are also assessed through parametric studies.

2. Finite element formulation of system

The shaking table tests of the two steel frames with and without fluid dampers linked were recently performed by the writers (Yang *et al.* 2002). The two steel frames with and without fluid dampers were kept elastic during the tests. To make use of the test results for the validation of the modeling procedure and the associated computer program in this study, two planar inelastic steel frames linked by a fluid damper are established based on the two steel frames tested (see Fig. 1).

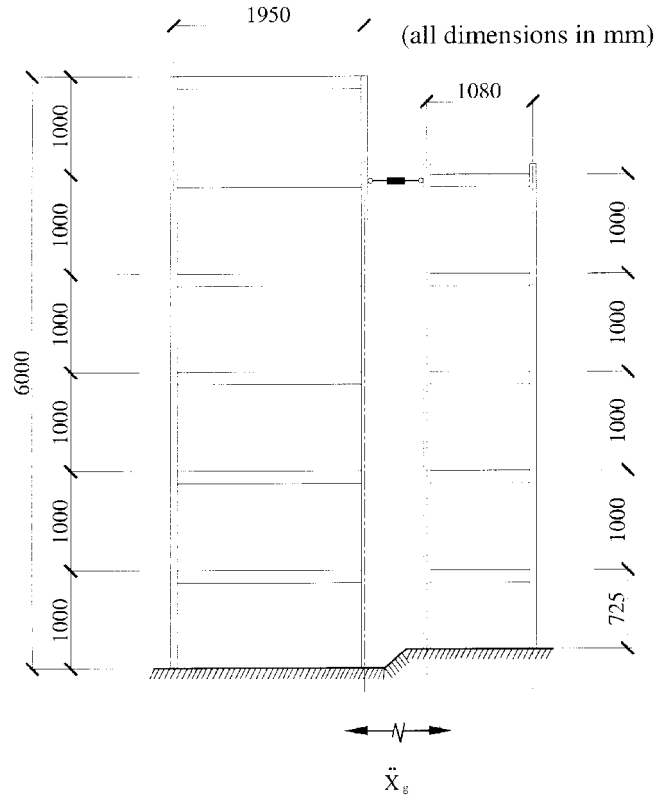


Fig. 1 Schematic model of adjacent buildings with fluid damper used in analysis

2.1 Element mass matrix

The beams and columns of the two planar steel frames are modeled by 2-D beam elements. The element has three degrees of freedom at each end: two translations and one rotation. The consistent mass concept with shear deflection effect included is employed to model the inertia force of the beam element. The element mass matrix in a local coordinate system possesses the following form (Yokoyama 1990).

$$\mathbf{M}^e = (\rho A + m)L \begin{bmatrix} 1/3 & & & & & & \\ 0 & A(r, \phi) & & & & & \text{symmetric} \\ 0 & C(r, \phi) & E(r, \phi) & & & & \\ 1/6 & 0 & 0 & 1/3 & & & \\ 0 & B(r, \phi) & D(r, \phi) & 0 & A(r, \phi) & & \\ 0 & -D(r, \phi) & -F(r, \phi) & 0 & -C(r, \phi) & E(r, \phi) & \end{bmatrix} \quad (1)$$

where ρ , m , A , L are, respectively, material density, additional mass per unit length, cross-section

area and length of beam element. Other functions in the above mass matrix are expressed as:

$$\begin{aligned}
 A(r, \phi) &= \frac{\frac{13}{35} + \frac{7}{10}\phi + \frac{1}{3}\phi^2 + \frac{6}{5}(r/L)^2}{(1 + \phi)^2} \\
 B(r, \phi) &= \frac{\frac{9}{70} + \frac{3}{10}\phi + \frac{1}{6}\phi^2 - \frac{6}{5}(r/L)^2}{(1 + \phi)^2} \\
 C(r, \phi) &= \frac{\left(\frac{11}{210} + \frac{11}{120}\phi + \frac{1}{24}\phi^2 + \left(\frac{1}{10} - \frac{1}{2}\phi\right)(r/L)^2\right)L}{(1 + \phi)^2} \\
 D(r, \phi) &= \frac{\left(\frac{13}{420} + \frac{3}{40}\phi + \frac{1}{24}\phi^2 - \left(\frac{1}{10} - \frac{1}{2}\phi\right)(r/L)^2\right)L}{(1 + \phi)^2} \\
 E(r, \phi) &= \frac{\left(\frac{1}{105} + \frac{1}{60}\phi + \frac{1}{120}\phi^2 + \left(\frac{2}{15} + \frac{1}{6}\phi + \frac{1}{3}\phi^2\right)(r/L)^2\right)L^2}{(1 + \phi)^2} \\
 F(r, \phi) &= \frac{\left(\frac{1}{140} + \frac{1}{60}\phi + \frac{1}{120}\phi^2 + \left(\frac{1}{30} + \frac{1}{6}\phi + \frac{1}{6}\phi^2\right)(r/L)^2\right)L^2}{(1 + \phi)^2} \tag{2}
 \end{aligned}$$

in which

$$r = \sqrt{\frac{I}{A}}, \text{ the radius of gyration of beam element.}$$

$$\phi = \frac{12EI}{GA_s L^2}, \text{ reflecting shear deflection effect.}$$

E , G , A_s , and I are the elastic modulus, shear modulus, effective shear area, and moment of inertia of beam element, respectively.

2.2 Linear-elastic element stiffness matrix

For a beam element in a completely linear-elastic state, the element stiffness matrix used in this study is expressed as:

the element. Three sets of integration points along the length of the element are arranged: one at each end section and one at the middle section. For each set (each cross section), five integration points are selected and located, respectively, at positions of $y = \pm 0.5 h$, $\pm 0.3 h$, and $0.0 h$ along the height of the cross-section, where h is the height of the cross section and y is the coordinate in the y -axis, one of the principle central axes of the cross section along the section height.

The inelastic element stiffness matrix changes with the motion of the steel frame under earthquake. For a given time, the inelastic element stiffness matrix is represented by its element tangent stiffness matrix. The general form of the tangent stiffness matrix for an elastic-plastic element is expressed as:

$$\mathbf{K}^e = \int_{Vol} \mathbf{B}^T \mathbf{D} \mathbf{B} d(Vol) \quad (4)$$

where \mathbf{B} is the strain-displacement matrix of the element; \mathbf{D} is the elastic-plastic stress-strain matrix of the element; and the term “ Vol ” denotes the volume of element.

For the 2-D beam element, the tangent stiffness matrix can be written as:

$$\mathbf{K}^e = \mathbf{K}_b^e + \mathbf{K}_s^e + \mathbf{K}_a^e \quad (5)$$

in which \mathbf{K}_b^e , \mathbf{K}_s^e , and \mathbf{K}_a^e are the matrices accounting for bending, shear, and axial deformation, respectively.

As each of these three matrices uses only one component of strain at one time, the integrand in Eq. (4) can be greatly simplified.

$$\mathbf{K}_b^e = \int_L (\mathbf{B}_x^B)^T \left[\int_{area} E(\varepsilon) y^2 d(area) \right] \mathbf{B}_x^B d(x) \quad (6)$$

$$\mathbf{K}_s^e = GA_s \int_L (\mathbf{B}^S)^T \mathbf{B}^S dx \quad (7)$$

$$\mathbf{K}_a^e = \int_L (\mathbf{B}^A)^T \left[\int_{area} E(\varepsilon) d(area) \right] \mathbf{B}^A d(x) \quad (8)$$

in which

$$\mathbf{B}_x^B = \frac{1}{L^2 + 12\phi} \left\{ 0, \quad \frac{12x}{L} - 6, \quad 6x - 4L - \frac{12\phi}{L}, \quad 0, \quad -\left(\frac{12x}{L} - 6\right), \quad 6x - 2L + \frac{12\phi}{L} \right\} \quad (9)$$

$$\mathbf{B}^S = \frac{6\phi}{L^2 + 12\phi} \left\{ 0, \quad -\frac{2}{L}, \quad -1, \quad 0, \quad \frac{2}{L}, \quad -1 \right\} \quad (10)$$

$$\mathbf{B}^A = \frac{1}{L} \{ 1, \quad 0, \quad 0, \quad -1, \quad 0, \quad 0 \} \quad (11)$$

$E(\varepsilon)$ is the current tangent modulus which can be found from the nonlinear stress-strain curve based on the current total strain ε and its history; the term “ $area$ ” denotes the cross section of the element; x is the coordinate in the x -axis, which is the longitudinal axis of the element. In the above

equations, the integration along the element length uses the three point Gauss rule while the integration over the cross-sectional area of the element is performed using the five point Gauss rule. The linear interpolation is used for determining the current tangent modulus at a Gauss point between the two integration points.

2.4 Stress and strain calculation

The stress and strain at any point of an element need to be calculated to facilitate the judgment of element state as well as to update the element tangent stiffness matrix. The trial elastic strain at any point in the beam element at the i^{th} step is given by:

$$\boldsymbol{\varepsilon}_i^{tr} = \boldsymbol{\phi}^b y + \boldsymbol{\varepsilon}^a - \boldsymbol{\varepsilon}_{i-1}^p \quad (12)$$

where $\boldsymbol{\phi}^b$ is the total curvature at the i^{th} step; $\boldsymbol{\varepsilon}^a$ is the total strain from the axial deformation at the i^{th} step; and $\boldsymbol{\varepsilon}_{i-1}^p$ is the plastic strain from the $(i-1)^{\text{th}}$ step. The total curvature and the total strain from the axial deformation are expressed as

$$\boldsymbol{\phi}^b = \mathbf{B}_x^B \mathbf{u}^B \quad (13)$$

$$\boldsymbol{\varepsilon}^a = \mathbf{B}^A \mathbf{u}^A \quad (14)$$

where \mathbf{u}^B and \mathbf{u}^A are the nodal displacement vector with non-zero bending component and axial component, respectively. The trial stress is then determined using the elastic modulus E .

$$\boldsymbol{\sigma}_i^{tr} = E \boldsymbol{\varepsilon}_i^{tr} \quad (15)$$

Three ingredients, namely, the yield criterion, the flow rule, and the hardening rule, should be now considered. The yield criterion determines the stress level at which yielding is initiated. The von Mises yield criterion is adopted in this study. The flow rule determines the direction of plastic straining and it is given as:

$$\Delta \boldsymbol{\varepsilon}_i^p = \lambda \left\{ \frac{\Delta Q}{\Delta \{ \boldsymbol{\sigma}_i^{tr} \}} \right\} \quad (16)$$

where λ is the plastic multiplier determining the amount of plastic straining; Q is a function of stress vector, termed plastic potential which determines the direction of plastic straining. $\{ \Delta \boldsymbol{\varepsilon}_i^p \}$ is the plastic strain increment. This study uses the associative flow rule and the yield function is selected as Q . The plastic strains thus occur in the direction normal to the yield surface. The hardening rule describes the change of the yield surface with progressive yielding so that the stress vector for subsequent yielding can be found. Kinematic hardening is used in this study, indicating that the yield surface remains constant in size and translates in the stress space with progressive yielding.

If the equivalent stress, calculated based on the stress vector and the von Mises yield criterion, exceeds the material yield stress, the plastic multiplier λ can be computed using the consistency condition, which ensures that the updated stress, strain and internal variables are on the yield surface

(Simo and Taylor 1985). The plastic strain increment is then obtained using the flow rule (Eq. 16). Finally, the current plastic strain is updated as

$$\boldsymbol{\varepsilon}_i^p = \boldsymbol{\varepsilon}_{i-1}^p + \Delta\boldsymbol{\varepsilon}_i^p \quad (17)$$

The current elastic strain vector and the current stress vector are computed by

$$\boldsymbol{\varepsilon}_i^e = \boldsymbol{\varepsilon}_i^{tr} - \Delta\boldsymbol{\varepsilon}_i^p \quad (18)$$

$$\boldsymbol{\sigma}_i = E\boldsymbol{\varepsilon}_i^e \quad (19)$$

2.5 Element damping matrix of damper

The fluid damper used to connect the two steel frames is a kind of viscous damper which can be modeled as a two-node damper element with uni-axial tension-compression capability of two degrees of freedom at each node (Soong and Dargush 1997). No damper mass is considered. The corresponding element damping matrix of damper can be given as

$$\mathbf{C}_d^e = c_d \begin{bmatrix} 1 & 0 & -1 & 0 \\ 0 & 0 & 0 & 0 \\ -1 & 0 & 1 & 0 \\ 0 & 0 & 0 & 0 \end{bmatrix} \quad (20)$$

where c_d is the damping coefficient of the damper.

2.6 Equation of motion of the system

Following the conventional finite element method to assemble all the element matrices, the equation of motion of the two steel frames linked by fluid dampers can be obtained as

$$\mathbf{M}\ddot{\mathbf{U}}(t) + \mathbf{C}\dot{\mathbf{U}}(t) + \mathbf{K}\mathbf{U}(t) = -\mathbf{M}\boldsymbol{\Gamma}\ddot{\mathbf{X}}_g(t) \quad (21)$$

where $\mathbf{U}(t)$, $\dot{\mathbf{U}}(t)$, and $\ddot{\mathbf{U}}(t)$ are, respectively, the displacement vector, the velocity vector, and the acceleration vector of the system relative to the ground; $\ddot{\mathbf{X}}_g(t)$ is the ground acceleration applied at the base of the two frames; $\boldsymbol{\Gamma}$ is the index vector; \mathbf{M} is the mass of the system; and \mathbf{K} is the elastic-plastic stiffness matrix of the system which is the function of $\mathbf{U}(t)$; and \mathbf{C} is the total damping matrix of the system which is the combination of the structural damping matrix and the damper damping matrix.

$$\mathbf{C} = \mathbf{C}_S + \mathbf{C}_D \quad (22)$$

The Rayleigh damping assumption is employed to derive the structural damping matrix if the system is in linear-elastic stage.

$$\mathbf{C}_S = a_0\mathbf{M} + a_1\mathbf{K} \quad (23)$$

in which a_0 and a_1 are the proportionality factors determined using the two given modal damping ratios. If the system enters into elastic-plastic stage, the structural damping matrix is determined by

$$\mathbf{C}_S = a_0\mathbf{M} \quad (24)$$

This assumption can avoid the unnecessary complexity due to the elastic-plastic stiffness matrix, and at the same time it is more reasonable to reflect the structural damping behavior in elastic-plastic stage. The damper damping matrix can be assembled from the element damping matrix of damper in the same way as the system stiffness matrix.

3. Numerical solution

A step-by-step numerical integration method using the Newmark- β method and the incremental modified Newton-Raphson iteration method are employed in this study to find the solution for inelastic seismic responses of adjacent buildings linked by fluid dampers.

3.1 Newmark- β method

The equation of motion of the damper-frame system (see Eq. 21) at the time t_i can be written in the incremental form.

$$\mathbf{M}\Delta\ddot{\mathbf{U}}_i + \mathbf{C}\Delta\dot{\mathbf{U}}_i + \mathbf{K}_i(\mathbf{U}, \dot{\mathbf{U}})\Delta\mathbf{U}_i = -\mathbf{M}\Gamma\Delta\ddot{\mathbf{X}}_{g,i} = \Delta\mathbf{R}_i \quad (25)$$

Following the Newmark- β method, the incremental pseudostatic equilibrium equation is

$$\bar{\mathbf{K}}_i\Delta\mathbf{U}_i = \Delta\bar{\mathbf{R}}_i \quad (26)$$

where

$$\bar{\mathbf{K}}_i = \mathbf{K}_i + \frac{\mathbf{M}}{\beta\Delta t^2} + \frac{\mathbf{C}}{2\beta\Delta t} \quad (27)$$

$$\Delta\bar{\mathbf{R}}_i = \Delta\mathbf{R}_i + \left(\frac{\mathbf{M}}{\beta\Delta t} + \frac{\mathbf{C}}{2\beta}\right)\dot{\mathbf{U}}_i + \frac{\mathbf{M}}{2\beta}\mathbf{U}_i - \mathbf{C}\Delta t\left(1 - \frac{1}{4\beta}\right)\ddot{\mathbf{U}}_i \quad (28)$$

$$\Delta t = t_{i+1} - t_i. \quad (29)$$

In this study, β is selected as 1/4. The incremental pseudostatic equilibrium Eq. (26) is solved using the incremental modified Newton-Raphson iteration method.

3.2 Modified Newton-Raphson iteration method

The general algorithm of the modified Newton-Raphson iteration method for the i^{th} time step of the incremental pseudostatic equilibrium equation can be summarized as follows:

- Initialize data

$$\mathbf{U}_i^0 = \mathbf{U}_i, \quad \bar{\mathbf{F}}_i^0 = \bar{\mathbf{F}}_i, \quad \mathbf{F}_i^0 = \mathbf{F}_i, \quad \bar{\mathbf{K}}_i^0 = \bar{\mathbf{K}}_i, \quad \Delta\bar{\mathbf{P}}_i^1 = \Delta\bar{\mathbf{R}}_i. \quad (30)$$

where $\bar{\mathbf{F}}_i$ and \mathbf{F}_i are, respectively, the equivalent restoring force vector related to the pseudostatic

equilibrium Eq. (26) and the real restoring force vector in the structural system at the beginning of the i^{th} time step.

- Carry out the iteration $j = 1, 2, 3, \dots$

$$\bar{\mathbf{K}}_i \Delta \bar{\mathbf{U}}_i^j = \Delta \bar{\mathbf{P}}_i^j \quad (31)$$

$$\mathbf{U}_i^j = \mathbf{U}_i^{j-1} + \Delta \mathbf{U}_i^j \quad (32)$$

$$\Delta \bar{\mathbf{F}}_i^j = \bar{\mathbf{F}}_i^j - \bar{\mathbf{F}}_i^{j-1} = \mathbf{F}_i^j - \mathbf{F}_i^{j-1} + (\bar{\mathbf{K}}_i - \mathbf{K}_i) \Delta \mathbf{U}_i^j \quad (33)$$

$$\Delta \bar{\mathbf{P}}_i^{j+1} = \Delta \bar{\mathbf{P}}_i^j - \Delta \bar{\mathbf{F}}_i^j \quad (34)$$

- Check convergence

If the $(j+1)^{\text{th}}$ iteration satisfies the following criteria, the iteration can be stopped.

$$\|\Delta \bar{\mathbf{P}}_i^{j+1}\| < \varepsilon_R P_{ref} \quad (35)$$

$$\|\Delta \mathbf{U}_i^{j+1}\| < \varepsilon_U U_{ref} \quad (36)$$

where ε_R and ε_U are the tolerances selected as 0.005 in this study; P_{ref} and U_{ref} are the reference values taken as $\|\Delta \bar{\mathbf{R}}_i\|$ and $\|\mathbf{U}_i\|$, respectively, in this study; $\|\bullet\|$ is a vector norm, a scalar measure of the magnitude of the vector.

3.3 Newton-Raphson restoring force vector

The Newton-Raphson restoring force for the element is:

$$\mathbf{F}_i^e = \int_{Vol} \mathbf{B}^T \mathbf{D} \boldsymbol{\varepsilon}_i^e d(Vol) \quad (37)$$

The meaning of each term in the above equation can be referred to sections 2.3 and 2.4. Analogous to the inelastic element stiffness matrix (section 2.3), the restoring force vector can be written as

$$\mathbf{F}_i^e = \mathbf{F}_b^e + \mathbf{F}_s^e + \mathbf{F}_a^e \quad (38)$$

in which \mathbf{F}_b^e , \mathbf{F}_s^e and \mathbf{F}_a^e are, respectively, restoring bending, shear, and axial force of the element. The subscript i has been left off for convenience.

$$\mathbf{F}_b^e = E \int_L (\mathbf{B}_x^B)^T \left[\int_{area} y \boldsymbol{\varepsilon}_i^e d(area) \right] dx \quad (39)$$

$$\mathbf{F}_s^e = GA_s \gamma_s \int_L (\mathbf{B}^S)^T dx \quad (40)$$

$$\mathbf{F}_a^e = E \int_L (\mathbf{B}^A)^T \left[\int_{area} \boldsymbol{\varepsilon}_i^e d(area) \right] dx \quad (41)$$

in which E is the elastic modulus and γ_s is the average shear strain due to shear forces in the element.

3.4 Incremental modified Newton-Raphson iteration method

It is noted that no any intermediate solution is in equilibrium except the final converged solution for each time step in the modified Newton-Raphson iteration process. However, for the elastic-plastic analysis with path-dependent nonlinear behavior, it is desirable to have some intermediate steps in equilibrium so as to follow the right load path. In this connection, this study divides each time step as five substeps and each of them is solved by the modified Newton-Raphson method. This is the so-called the incremental modified Newton-Raphson iteration method.

4. Linear-elastic seismic response and comparison

The two planar steel frames linked by linear fluid dampers shown in Fig. 1 are actually the simplified model for the two steel frames recently tested by the writers on the shaking table (Yang *et al.* 2002). The two test steel frames of a 1:4 length scale were designed as a symmetric 6-story frame of 6 m high and a symmetric 5-story frame of 5 m high (see Fig. 3). The test case used in this study for the comparison is that the two steel frames were aligned in the x -direction and linked by linear fluid dampers in parallel. They were mounted on a 4 m \times 4 m earthquake simulator and subjected to the ground acceleration in the x -direction only. Under these conditions, the two test steel frames linked by fluid dampers can be accordingly modeled as two planar steel frames linked by fluid dampers for the convenience of computation. The geometric properties of the two planar steel frames are listed in Table 1. The elastic modulus E , plastic modulus E_p , and yield stress f_y of the materials are 206 GPa, 2.06 GPa, and 215 MPa respectively. The Poisson's ratio μ and the shear modulus G are taken as 0.3 and 79 GPa, respectively. The first three natural frequencies of 6-story frame are 1.86 Hz, 5.86 Hz, and 9.77 Hz and the first three natural frequencies of 5-story frame are 3.42 Hz, 10.35 Hz, and 16.02 Hz. The damping coefficient of fluid damper c_d is about 15.41 N.s/mm. The first two modal damping ratios of either frame, used to constitute the structural damping matrix, are taken as 1%. The ground acceleration is the El Centro 1940 N-S ground motion of 0.2 g peak acceleration and 26 seconds duration inputted in the x -direction only.

The test results showed that the two frames in this test case were in completely linear-elastic stage no matter whether the fluid dampers were installed or not. The measured maximum strain was 722 $\mu\epsilon$ in the 6-story frame and 405 $\mu\epsilon$ in the 5-story frame without fluid dampers. With the two parallel dampers connected at the 5th floor of both the frames, the maximum strain was measured as 402 $\mu\epsilon$ in the 6-story frame and 196 $\mu\epsilon$ in the 5-story frame while the yield strain of steel used in the test was about 1044 $\mu\epsilon$.

Table 1 Geometric properties of structural elements

Frame (1)	Element (2)	A (m ²) (3)	I (m ⁴) (4)
6-story frame	Beam	1.569×10^{-3}	3.885×10^{-6}
	Column	1.433×10^{-3}	3.281×10^{-7}
5-story frame	Beam	1.569×10^{-3}	3.885×10^{-6}
	Column	1.433×10^{-3}	3.281×10^{-7}

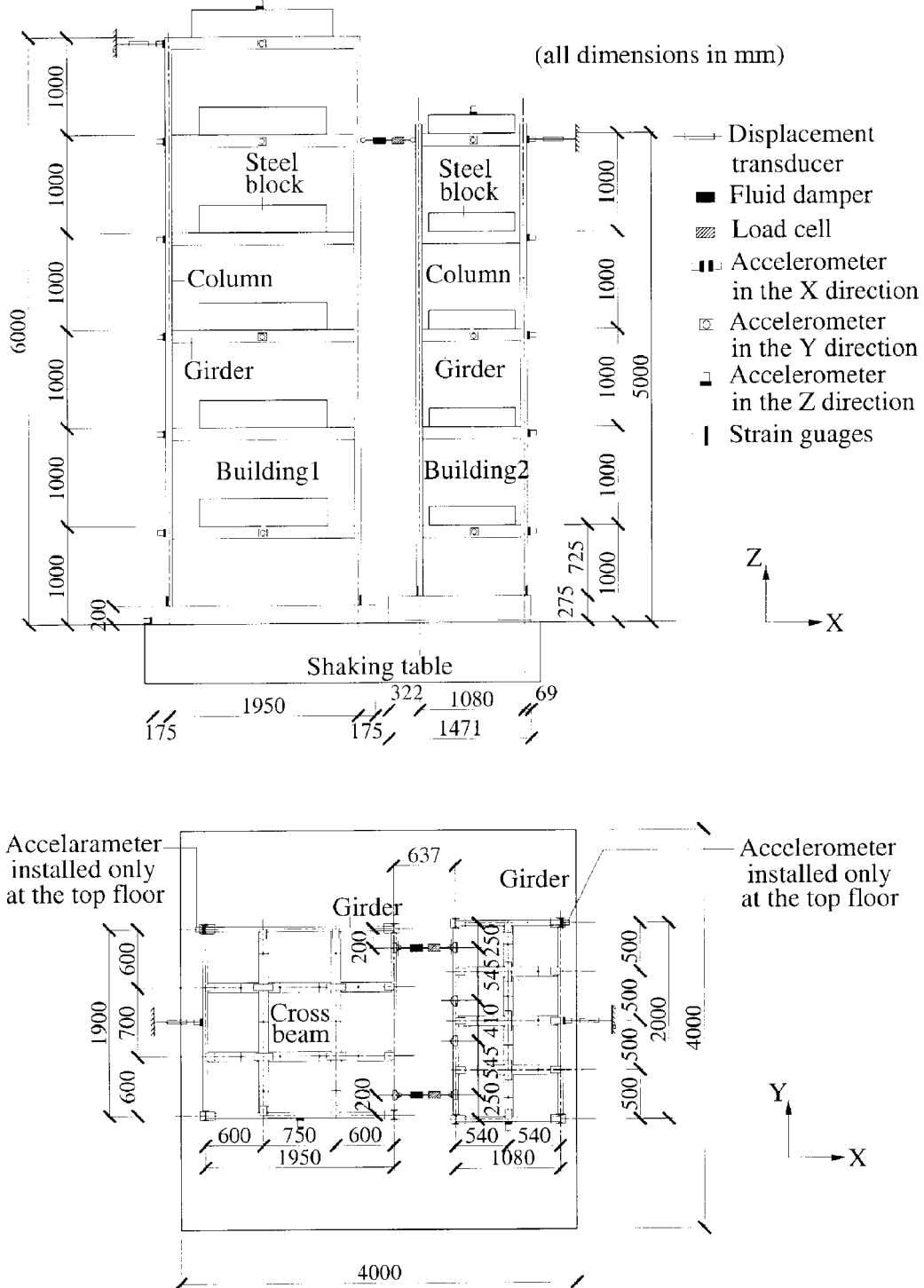


Fig. 3 Configuration and instrumentation of adjacent buildings with fluid damper in shaking table test

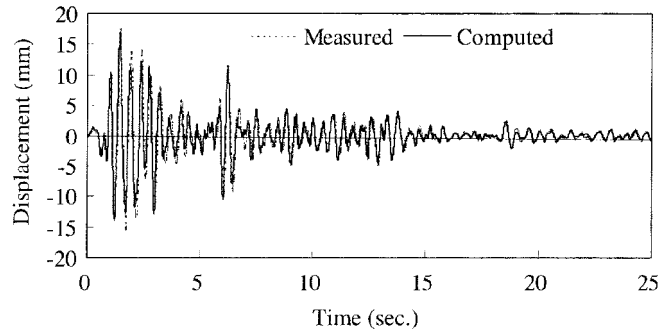


Fig. 4 Comparison of time-history of linear-elastic displacement response at top floor of 6-story frame

Displayed in Fig. 4 are the time-histories of top-floor horizontal displacement response of the 6-story frame with one fluid damper (referring to the computer model) installed at the 5th floor and connected to the 5-story frame. The computed time-history is compared with the measured time-history and the comparison is satisfactory. Fig. 5(a) depicts the variation of the maximum horizontal displacement response of the 6-story frame with height, in which one fluid damper is installed at the 5th floor and linked to the 5-story frame. Fig. 5(b) shows the same quantity but without fluid dampers. It is seen that the computed results are close to the measured results. These results demonstrate that the linear-elastic computer model used in this study is accurate enough and can be used for parametric studies. The comparative results also indicate that the effect of geometric non-linearity on the linear-elastic seismic response of steel frames is insignificant. Although this comparison is performed for the linear-elastic steel frames, the good agreement implies that the computed model and numerical solution used in this study may be used for the elastic-plastic analysis of two steel frames linked by fluid dampers.

For the case in which the 6-story frame and the 5-story frame are linked together at the 5th floor through one fluid damper, the effect of damper damping coefficient on the seismic response reduction is investigated using the computational model. Fig. 6 shows that the variation of displacement response reduction ratio with the normalized damper damping coefficient. The displacement response reduction ratio is defined as the RMS response of the frame with control to

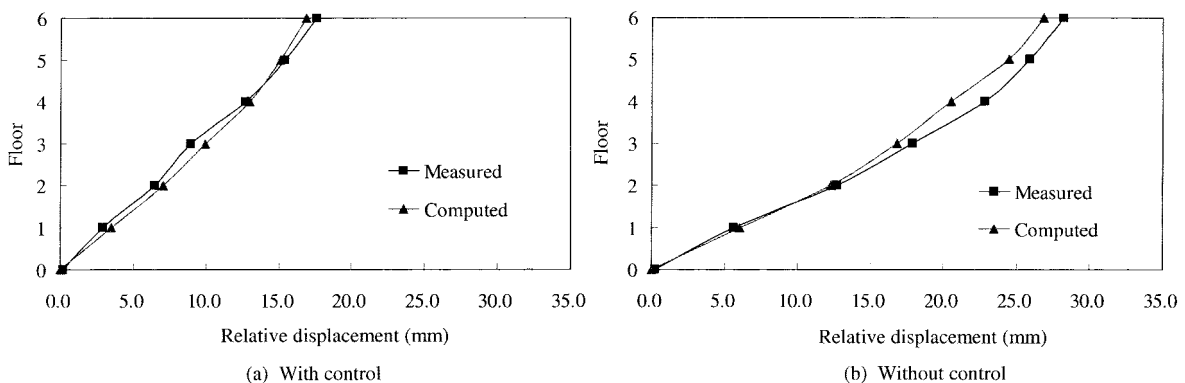


Fig. 5 Comparison of maximum linear-elastic floor displacement response of 6-story Frame

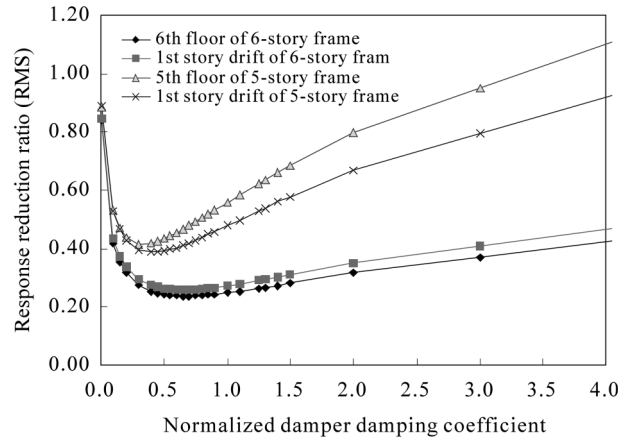


Fig. 6 Variation of linear-elastic RMS response reduction ratio with damper damping coefficient

the same quantity of the frame without control. The normalized damper damping coefficient is defined as the damper damping coefficient divided by the damper damping coefficient used in the test. It is seen that the variation of the 6th floor response reduction ratio of the 6-story frame with the normalized damper damping coefficient is similar to that of the first story drift of the 6-story frame. However, the variation of the 6th floor response reduction ratio of the 6-story frame is different from that of the 5th floor of the 5-story frame. The seismic response of the 6-story frame is not very sensitive to the damper damping coefficient if it is larger than 0.4. The seismic response of the 5-story frame is, however, sensitive to the damper damping coefficient. The optimal normalized damper damping coefficient is about at 0.65 for the 6-story frame with the RMS response reduction ratio about 23.8% for the top floor displacement response and 25.9% for the first story drift. For the 5-story frame, the optimal normalized damper damping coefficient is about 0.4 with the RMS response reduction ratio about 41.9% for the top floor displacement response and 38.8% for the first story drift. Fig. 7 displays the time histories of top-floor displacement response of the 6-story frame without fluid damper and with the optimal fluid damper. The optimal fluid damper is very effective during the whole duration of the ground motion. Apart from the significant reduction of RMS response, the maximum displacement response is also reduced by 42%.

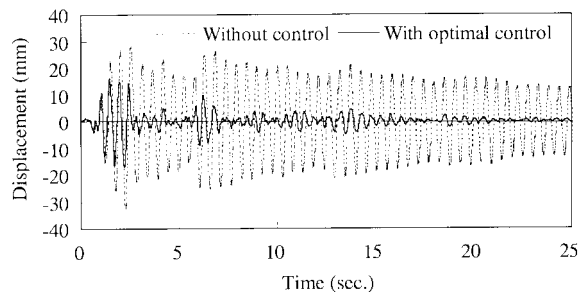


Fig. 7 Time-histories of linear-elastic displacement responses at top floor of 6-story frame with and without control

5. Elastic-plastic seismic response

The elastic-plastic seismic responses of the two steel frame models without and with one fluid damper installed at the 5th floor are computed by changing the peak acceleration of the El Centro ground motion. The basic peak acceleration is selected as 0.2 g as used in the linear-elastic analysis. The seismic intensity multipliers of the basic peak acceleration used in the elastic-plastic analysis are taken from 1 to 6 for the case without control and from 1 to 8 for the case with control. The ground acceleration selected here is referred to the model frame rather than the prototype frame. The use of large ground acceleration will provide a clear picture of the elastic-plastic behavior of the concerned steel frames.

5.1 Maximum displacement response profile

Plotted in Fig. 8(a) is the variation of the normalized maximum horizontal displacement response of the 6-story frame with the height for a number of the seismic intensity multipliers and for the case without control. For a given seismic intensity multiplier, the normalized maximum horizontal displacement response at the i^{th} floor is defined as the maximum horizontal displacement at the i^{th} floor divided by the maximum horizontal displacement at the top floor. It is seen that the steel frame is a shear type of structure. When the seismic intensity multiplier ranges from 1 to 3, the normalized maximum horizontal displacement profiles are almost overlapped, which indicates the frame almost in the linear-elastic status. With the seismic intensity multiplier increasing from 4, the plastic deformation of the frame becomes larger and larger. Fig. 8(b) also displays the variation of the normalized maximum horizontal displacement response of the 6-story frame but this is for the case with control. It is interesting to see that because of the installation of fluid damper, the displacement profiles overlaps for the seismic intensity multiplier ranging from 1 to 5. Only starting from the multiplier of 6, the frame exhibits plastic deformation. Comparing with the multiplier of 4 for the case without control, one may see the significant improvement of seismic resistant capacity of the frame with the installation of fluid damper. The type of shear structure, however, is still kept with the fluid damper.

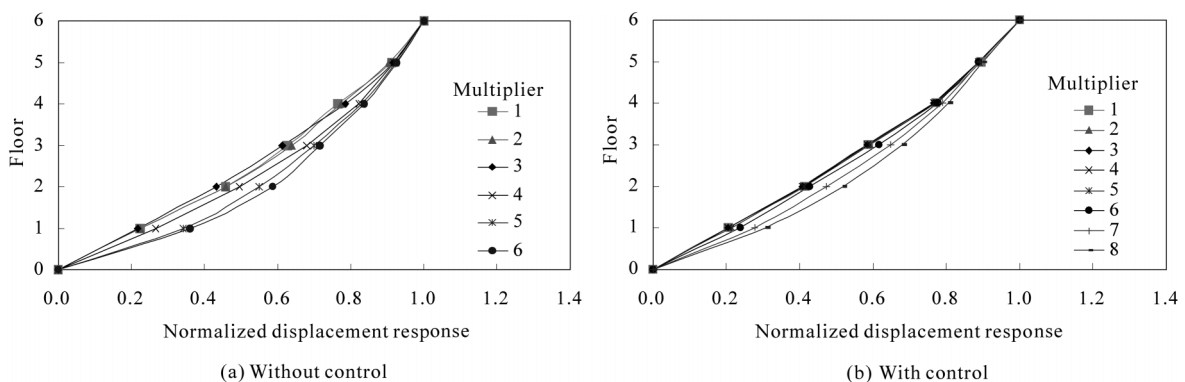


Fig. 8 Variation of normalized displacement response of 6-story frame with height

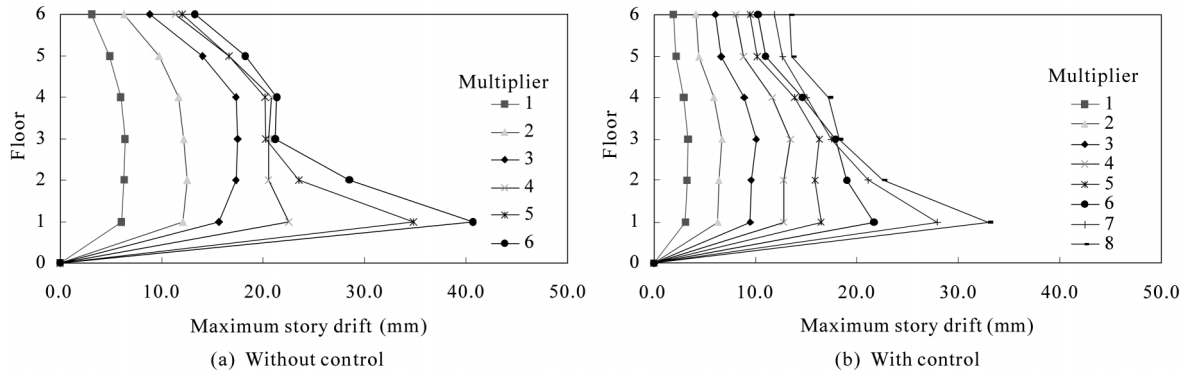


Fig. 9 Variation of maximum story drift of 6-story frame with height

5.2 Maximum story drift profile

To view the distribution of elastic-plastic deformation of the steel frame along the height, the maximum story drifts of the two steel frames with and without fluid dampers are computed. Figs. 9(a) and 9(b) display the maximum story drifts of the 6-story frame without and with the fluid damper at the 5th floor, respectively, for a series of the seismic intensity multiplier. It is seen from Fig. 9(a) that when the multiplier increases from 4, the plastic deformation appears in the first story and the first story drift gets larger and larger. This illustrates that the first story of the 6-story frame is a weak story. With the installation of the fluid damper at the 5th floor, the occurrence of plastic deformation is delayed to the multiplier of 6 but it still occurs at the first story. Under the same ground acceleration, the story drifts become much smaller in the control case than in the case without control, as shown in Figs. 9(a) and 9(b). The computed results show, however, that for the 5-story frame, the plastic deformation occurs at the second story first for both cases with and without control. This is because the first story height is less than the other stories. The second story is thus the weak story of the 5-story frame.

5.3 Hysteretic characteristics

To confirm the occurrence of plastic deformation and to view the development of elastic-plastic deformation under increasing peak ground acceleration, the hysteretic loops of the column end moment vs. the story drift are computed for each story of each frame for a series of seismic intensity multipliers. Figs. 10(a) and 10(b) show the $M-\Delta$ hysteretic loops of the first story of the 6-story frame without control for the seismic intensity multiplier of 1 and 4, respectively. Clearly, for the multiplier of 1, i.e., under the 0.2 g peak ground acceleration, the $M-\Delta$ curve appears in a straight line, indicating the first story is in the perfect linear-elastic status. For the multiplier of 4, a clear bi-linear $M-\Delta$ hysteretic loop appears in the first story. The bi-linear $M-\Delta$ hysteretic loop comes from the bi-linear stress-strain relationship for the material used in this study. Comparing Fig. 10(a) with Fig. 10(b), one may see that the column end moment and the story drift of the first story are much larger for the multiplier of 4 than for the multiplier of 1.

With the installation of fluid damper at the 5th floor, the $M-\Delta$ curve of the first story of the 6-story frame appears in a straight line for the seismic intensity multiplier of 4 (see Fig. 10c). This

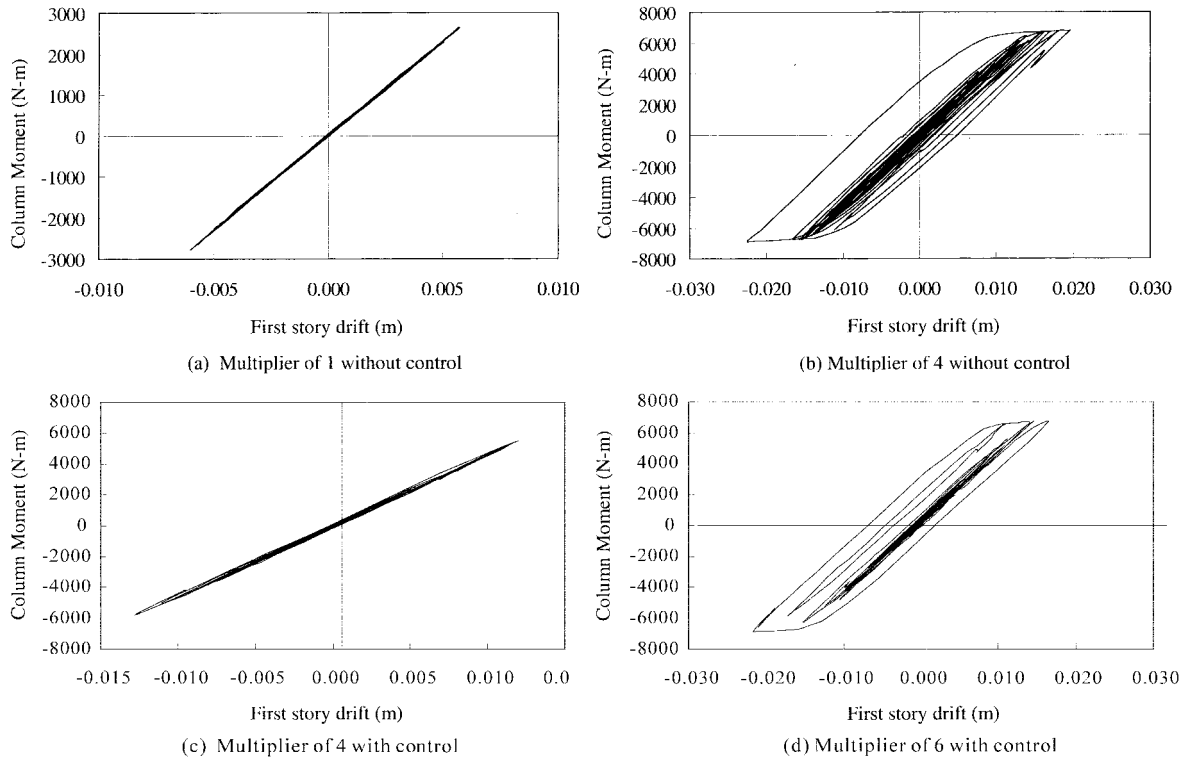


Fig. 10 Hysteretic loops of first story of 6-story frame

demonstrates that the installation of fluid damper postpones the occurrence of the plastic deformation. The column end moment and the story drift are also reduced significantly, compared with those in Fig. 10(b). When the seismic intensity multiplier reaches above 6, the plastic deformation occurs in the first story of the frame with control, as shown in Fig. 10(d). It is found that if the plastic deformation is developed in one story, the maximum column end moment remains almost unchanged while the story drift still increases with increasing ground motion intensity.

5.4 Optimal damper damping coefficient

To further evaluate the effectiveness of fluid damper in reducing the elastic-plastic seismic response of the steel frame, the RMS displacement response reduction ratios are computed for each floor of each frame against the normalized damper damping coefficient. The fluid damper is installed at the 5th floor and the seismic intensity multiplier is 6. Some of the computed results are shown in Fig. 11. It is seen that the variation of the 5th floor response reduction ratio of the 5-story frame with the normalized damper damping coefficient is similar to that of the first story drift of the 5-story frame. However, the variation of the 5th floor response reduction ratio of the 5-story frame is different from that of the 6th floor of the 6-story frame. The seismic response of the 6-story frame is not very sensitive to the damper damping coefficient if it is larger than 0.4. The seismic response of the 5-story frame is, however, sensitive to the damper damping coefficient. This is similar to the linear-elastic steel frames, as shown in Fig. 6. The optimal normalized damper damping coefficient

is about at 0.7 for the 6-story frame with the RMS response reduction ratio about 39.1% for the top floor displacement response and 31.9% for the first story drift. For the 5-story frame, the optimal normalized damper damping coefficient is about 0.3 with the RMS response reduction ratio about 37.0% for the top floor displacement response and about 0.4 with the RMS response reduction ratio about 40.7% for the first story drift.

Comparing with Fig. 6 for the linear-elastic case, one may observe that the effectiveness of the fluid damper in reducing elastic-plastic seismic response is lower than in reducing linear-plastic seismic response for the 6-story frame but remains almost the same for the 5-story frame. The optimal damper damping coefficients for reducing the elastic-plastic seismic response of the steel frames change slightly compared with those for reducing the linear-elastic seismic response. This feature is favorable for the practical use of the fluid damper.

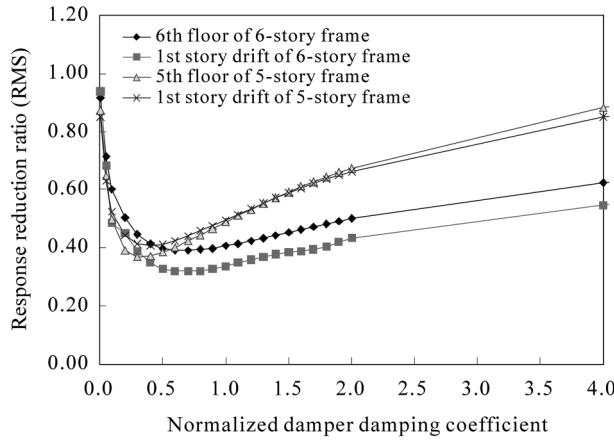


Fig. 11 Variation of inelastic RMS response reduction ratio with damper damping coefficient

5.5 Comparison of response time history

Fig. 12 depicts the time histories of top-floor displacement response of the 6-story frame without fluid damper and with the optimal fluid damper for the seismic intensity multiplier of 6. Both are elastic-plastic response time-histories. The effectiveness of fluid damper in reducing either the RMS

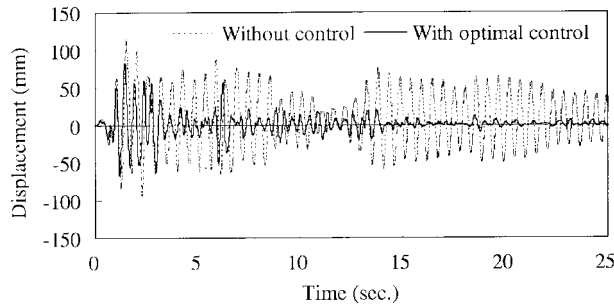


Fig. 12 Time-histories of inelastic displacement responses at top floor of 6-story frame with and without control

elastic-plastic response or the maximum elastic-plastic response is clearly demonstrated. Compared with Fig. 7 for the linear-elastic seismic response time-histories, it is also seen that the effectiveness of the fluid damper in reducing elastic-plastic seismic response is lower than in reducing linear-elastic seismic response. This is because the intrinsic energy dissipation capacity of the frames in the inelastic range is higher than in the elastic range.

5.6 Effects of frequency ratio

To assess the influence of the fundamental frequency ratio of the two frames on the control performance, the fundamental frequency of the 5-story frame is adjusted from 3.42 Hz to 2.74 Hz. Thus, the fundamental frequencies of the two frames are more close to each other than before and the new frequency ratio becomes 1:0.8 compared with the previous frequency ratio of 1: 0.54. According to the optimal damper damping coefficients obtained from Fig. 6 and Fig. 11 for the frames with the frequency ratio of 1:0.54, the damper damping coefficient of $0.5c_d$ namely 7.70 N.s/mm, is used for the present matter. The computed maximum story drifts of the 6-story frame with the fluid damper at the 5th floor are displayed in Fig. 13 for the frequency ratios of 1:0.54 and 1:0.8 and for the seismic intensity multipliers of 1 and 6. It is seen that the effectiveness of the fluid damper is deteriorated significantly when the frequency ratio is changed from 1:0.54 to 1:0.8 no matter what the multiplier is. By taking the 1st story drift of the 6-story frame as an example, the maximum story drift ratio (the maximum story drift with control over the maximum story drift without control) is increased from 0.45 to 0.85 for the seismic intensity multiplier of 1 and from 0.50 to 0.86 for the seismic intensity multiplier of 6 when the frequency ratio is increased from 1:0.54 to 1:0.8. It seems that the fluid damper is more effective when the fundamental frequencies of the two frames are far apart. However, it should be pointed out that the damper damping coefficient used in the computation may not be the optimal damping coefficient for the two frames of the frequency ratio of 1:0.8. The control performance could be enhanced for the case of the frequency ratio of 1:0.8 if the damper damping coefficient is increased.

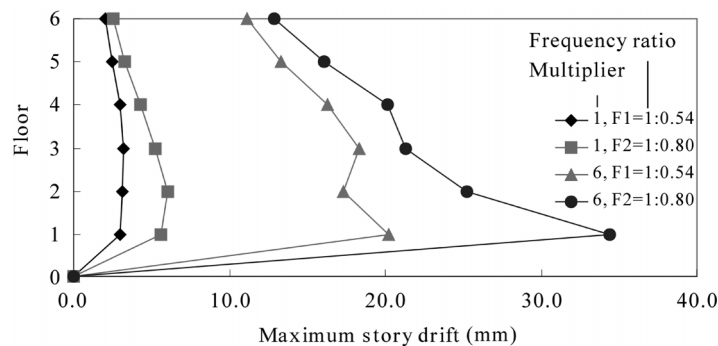


Fig. 13 Variation of maximum story drift of 6-story frame with height for different frequency ratios

5.7 Effects of structural damping ratio

To show the influence of the structural damping ratio of the two frames on control performance, the structural damping ratio of 5% is applied to the two frames with the multiplier of either 1 or 6.

The frequency ratio of the two frames remains at 1:0.54. The computed maximum story drifts of the 6-story frame without and with the fluid damper at the 5th floor are plotted in Fig. 14 and listed in Table 2 for the structural damping ratios of 1% and 5% and for the seismic intensity multipliers of 1 and 6. Listed in Table 2 is also the response ratio of the maximum story drift with control to the maximum story drift without control for the frame for different structural damping ratios and different seismic intensity multipliers. It is seen that when the structural damping ratio is increased from 1% to 5%, all the maximum story drifts are reduced for the frame either with or without control and with either the multiplier of 1 or 6. It is also seen that except for the first floor, the

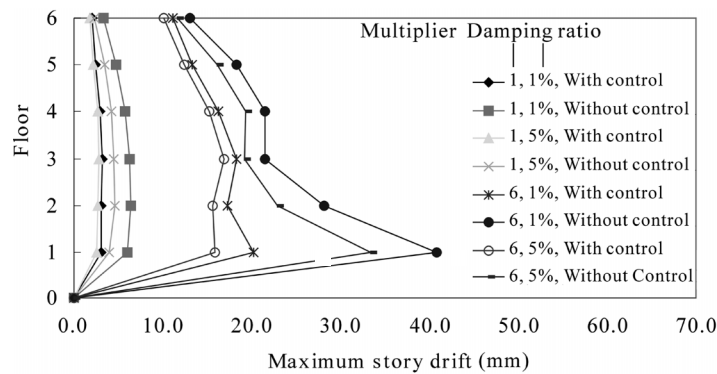


Fig. 14 Variation of maximum story drift of 6-story frame with height for different structural damping ratios

Table 2 Maximum story drifts and response ratios of the 6-story frame

Location	Multiplier	Story Drift (1% Damping Ratio)		Response Ratio (4)/(3)	Story Drift (5% Damping Ratio)		Response Ratio (7)/(6)
		Without Control (mm)	With Control (mm)		Without Control (mm)	With Control (mm)	
(1)	(2)	(3)	(4)	(5)	(6)	(7)	(8)
1 st Story	1	5.99	3.01	0.50	4.02	2.59	0.64
	6	40.8	20.2	0.50	33.4	15.8	0.47
2 nd Story	1	6.43	3.10	0.48	4.64	2.64	0.57
	6	28.2	17.3	0.61	22.9	15.6	0.68
3 rd Story	1	6.26	3.22	0.51	4.43	2.86	0.65
	6	21.4	18.3	0.86	19.2	16.9	0.88
4 th Story	1	5.77	2.98	0.52	4.23	2.65	0.63
	6	21.5	16.3	0.76	19.4	15.2	0.78
5 th Story	1	4.73	2.48	0.52	3.41	2.17	0.64
	6	18.3	13.3	0.73	16.1	12.4	0.77
6 th Story	1	3.27	2.00	0.61	2.34	1.77	0.76
	6	13.1	11.1	0.85	11.7	10.1	0.86

response ratio of the frame with the multiplier of 6 is higher than that with the multiplier of 1, which indicates that the fluid damper is more effective for the frame under small earthquake event than under large earthquake event. Also except for the first floor, the response ratio is higher for the frame with higher structural damping ratio no matter what the multiplier is. This indicates that the fluid damper is more effective in the case of smaller structural damping ratio. However, the above observations do not apply for the first floor. The response ratio of the first floor with the multiplier of 6 is the same as or less than that with the multiplier of 1. Furthermore, for the frame with the multiplier of 6, the response ratio of the first floor with higher structural damping ratio is smaller than that with lower structural damping ratio. It is noted that the first floor is the weakest floor of the 6-story frame. Thus, the first floor of the controlled frame of higher structural damping ratio enters inelastic stage far less than that of lower structural damping ratio, resulting in a better control performance.

6. Conclusions

Elastic and inelastic seismic responses of adjacent buildings with and without fluid dampers connected have been investigated using plastic-zone beam elements and nonlinear finite element approach. Computed linear elastic seismic responses of the two steel frames with and without fluid dampers under moderate seismic events were compared with the experimental results obtained from shaking table tests, and a satisfactory comparison was achieved. The elastic-plastic seismic responses of the two steel frames with and without fluid dampers were extensively computed and the fluid damper performance on controlling inelastic seismic response of the two steel frames was assessed. The results showed that not only in linear elastic stage but also in inelastic stage, the seismic resistant performance of the two steel frames could be significantly enhanced. The optimal damper damping coefficients for reducing the elastic-plastic seismic response of the steel frames changed only slightly compared with those for reducing the linear-elastic seismic response. The seismic response reduction of the 6-story steel frame was not sensitive to damper damping coefficient if the coefficient exceeded a certain value but this was not true for the 5-story steel frame. The computed horizontal floor displacement responses, the story drifts, and the hysteretic loops of the steel frames under increasing peak ground acceleration clearly demonstrated the occurrence and distribution of plastic deformation. The installation of fluid damper postponed the occurrence of the plastic deformation but did not change the distribution pattern of the plastic deformation.

The effects of the fundamental frequency ratio and structural damping ratio of the two steel frames on the damper performance were also examined. It was found that the control performance was better for the frame with the frequency ratio of 1:0.54 than that with the frequency ratio of 1:0.8. It was also found that except for the first story, the control performance was better for all the stories of the frame with lower structural damping ratio. It should be pointed out that all the above conclusions were made based on the two frames investigated. The general procedure for determining the optimum damper damping ratio and the effectiveness of the fluid damper based on the dynamic properties of two adjacent buildings for the design purpose is under investigation by simplifying the two adjacent buildings as a two-degree-of-freedom system.

Acknowledgements

The writers are grateful for the financial supports from the Hong Kong Polytechnic University through its Area of Strategic Development Programme in Structural Control and Intelligent Buildings to the first writer and the National Natural Science Foundation of China through an NNSF grant (50025821) to the third writer.

References

- Christenson, R.E., Spencer, B.F. and Johnson, E.A. (1999), "Coupled building control using active and smart damping strategies", *Proc. 5th Int. Conf. on Application of Artificial Intelligence to Civil and Struct. Engng.*, Oxford, UK, 187-195.
- Klein, R.G. and Healy, M.D. (1985), "Semi-active control of wind induced oscillations in structures", *Proc. 2nd Int. Conf. on Struct. Control*, Ontario, Canada, 354-369.
- Kobori, T., Yamada, T., Takenaka, Y., Maeda, Y. and Nishimura, I. (1988), "Effect of dynamic tuned connector on reduction of seismic response: application to adjacent office buildings", *Proc. 9th World Conf. On Earthquake Engng.*, **5**, Tokyo-Kyoto, Japan, 773-778.
- Luco, J.E. and De Barros, F.C.P. (1998), "Optimal damping between two adjacent elastic structures", *Earthq. Engng. Struct. Dyn.*, **27**, 649-659.
- Pi, Y.L. and Trahair, N.S. (1994), "Nonlinear inelastic analysis of steel beam-columns. I: theory", *J. Struct. Engng.*, ASCE, **120**(7), 2041-2061.
- Seto, T. and Matsumoto, Y. (1996), "A structural vibration control method of flexible buildings in response to large earthquakes and strong winds", *Proc. 2nd Int. Workshop on Struct. Control*, Hong Kong, 490-496.
- Simo, J.C. and Taylor, R.L. (1985), "Consistent tangent operations for rate-independent elastoplasticity", *Comp. Methods Appl. Mech. Engng*, **48**, 101-118.
- Soong, T.T. and Dargush, G.F. (1997), *Passive Energy Dissipation Systems in Structural Engineering*, John Wiley & Sons, Chichester, England.
- Xu, Y.L., Zhan, S., Ko, J.M. and Zhang, W.S. (1999) "Experimental investigation of adjacent buildings connected by fluid damper", *Earthq. Engng. Struct. Dyn.*, **29**, 557-575.
- Yamada, Y., Ikawa, N., Yokoyama, H. and Tachibana, E. (1994), "Active control of structures using the joint member with negative stiffness", *Proc. 1st World Conf. On Struct. Control*, **2**, Los Angeles, California, USA, TP2: 41-49.
- Yang, Z., Xu, Y.L. and Lu, X.L. (2002), "Experimental study of seismic adjacent buildings with fluid dampers", *J. Struct. Engng.*, ASCE, **129**(2), 197-205.
- Yokoyama, T. (1990), "Vibrations of a hinging Timoshenko beam under gravity", *J. Sound Vib.*, **141**(2), 245-258.
- Zhang, W.S. and Xu, Y.L. (1999), "Dynamic characteristics and seismic response of adjacent buildings linked by discrete dampers", *Earthq. Engng. Struct. Dyn.*, **28**, 1163-1185.